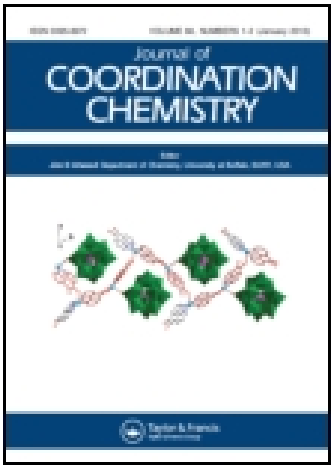

Journal of Coordination Chemistry
Publication details, including instructions for authors and subscription information:
http://www.tandfonline.com/loi/gcoo20

Synthesis, characterization, crystal structure, and DNA binding of two copper(II)-hydrazone complexes

Madshusudan Nandy[a], David L. Hughes[b], Georgina M. Rosair[c], Raj Kumar Bhubon Singh[d] & Samiran Mitra[a]

[a] Department of Chemistry, Jadavpur University, Kolkata, India

[b] School of Chemistry, University of East Anglia, Norwich, UK

[c] Department of Chemistry, School of Engineering and Physical Sciences, Heriot-Watt University, Edinburgh, UK

[d] Department of Chemistry, Manipur University, Imphal, India

Accepted author version posted online: 11 Sep 2014.Published online: 07 Oct 2014.

To cite this article: Madshusudan Nandy, David L. Hughes, Georgina M. Rosair, Raj Kumar Bhubon Singh & Samiran Mitra (2014) Synthesis, characterization, crystal structure, and DNA binding of two copper(II)-hydrazone complexes, Journal of Coordination Chemistry, 67:20, 3335-3353, DOI: 10.1080/00958972.2014.964697

To link to this article: http://dx.doi.org/10.1080/00958972.2014.964697

Journal of Coordination Chemistry, 2014
Vol. 67, No. 20, 3335–3353, http://dx.doi.org/10.1080/00958972.2014.964697

Synthesis, characterization, crystal structure, and DNA binding of two copper(II)–hydrazone complexes

MADSHUSUDAN NANDY†, DAVID L. HUGHES‡, GEORGINA M. ROSAIR§, RAJ KUMAR BHUBON SINGH¶ and SAMIRAN MITRA*†

†Department of Chemistry, Jadavpur University, Kolkata, India
‡School of Chemistry, University of East Anglia, Norwich, UK
§Department of Chemistry, School of Engineering and Physical Sciences, Heriot-Watt University, Edinburgh, UK
¶Department of Chemistry, Manipur University, Imphal, India

(*Received 9 October 2013; accepted 27 August 2014*)

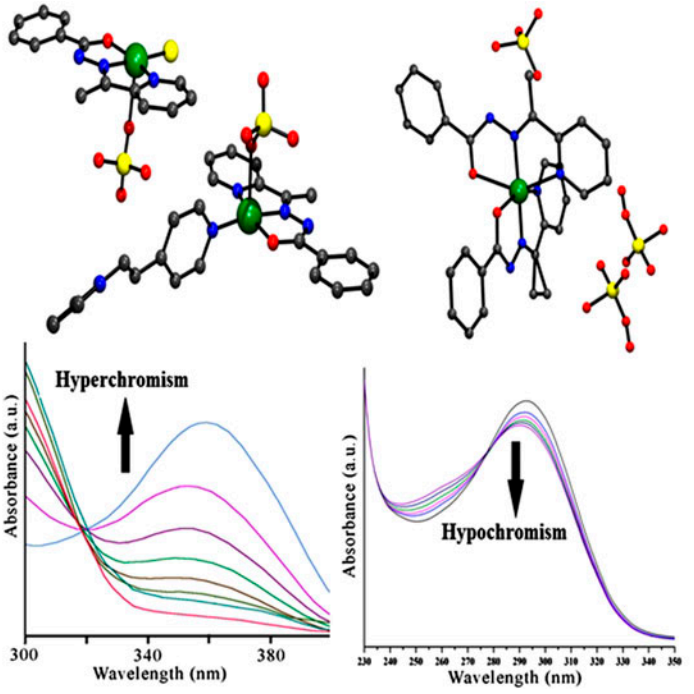

Two new Cu(II)–hydrazone complexes, $[Cu(L)(Hbpe)ClO_4]\cdot ClO_4\cdot[Cu(L)Cl]$ (**1**) and $[Cu(HL)_2]\cdot 1.5ClO_4\cdot 0.5OH$ (**2**) (where HL = (E)-N′-(1-(pyridine-2-yl)ethylidene)benzohydrazide and bpe = *trans*-1-(2-pyridyl)-2-(4-pyridyl)ethylene), have been synthesized and characterized by physicochemical methods. The structures of the complexes have been established by single-crystal X-ray

*Corresponding author. Email: smitra@chemistry.jdvu.ac.in

diffraction direct methods, which reveal that the metal ions have distorted square-pyramidal and square-planar geometries in **1**, and a distorted octahedral geometry in **2**. DNA binding of HL, **1**, and **2**, performed by UV–vis titration in tris-buffer medium, yielded binding constants, which are 9.5×10^3, 1.88×10^4, and 4.66×10^4 M^{-1}, respectively. Viscosity measurements suggest a surface or groove-binding mode of interaction between CT-DNA with HL, **1**, and **2**.

Keywords: Copper(II)–hydrazone complex; Crystal structure; DNA binding; Electrochemistry; EPR

1. Introduction

Metal complexes have interest in clinical biology for their capabilities to bind DNA under physiological conditions [1–3]. Many metal complexes have potential application as anticancer drugs by inhibiting the growth of tumor cells through binding to DNA, thereby blocking its replication. Thus, understanding DNA-binding affinity of metal complexes is the basis for designing efficient antitumor drugs [4, 5]. Since the discovery of the antitumor activity of cisplatin, numerous mono-nuclear platinum(II) complexes have been synthesized and their anticancer activities are carefully evaluated on appropriate biological models [6]. Most show remarkable cytotoxicity with low selectivity. Moreover, platinum forms covalent bonds to N7 of adjacent purine bases and denatured DNA helical structure. Therefore, design and synthesis of new metal-based anticancer drugs that exhibit less toxicity, enhanced selectivity, and non-covalent DNA binding are of interest [7]. Non-covalent DNA interactions include intercalative, electrostatic, and groove binding. Studies have provided significant insight into the minor groove binding of small molecules, which possess hydrogen bonding or van der Waals interactions. Moreover, it also depends on the coordination geometry of the metal ion and donor type of the ligand [8].

The chemistry of copper complexes with biological ligands [9] is one of the fascinating topics in modern research due to their attractive structural, catalytic, electrochemical, and magnetic properties [10]. Moreover, copper is a vital trace element and plays an important role as a cofactor for many metalloenzymes, and is also essential for various biological courses of actions [11, 12]. Moreover, copper complexes have interest due to their low cost, ease of synthesis, and increasing number of complexes with potential impact in medicinal applications [13–17]. Copper(II) complexes containing heterocyclic bases have been comprehensively investigated for their strong interactions with DNA and cytotoxic activity [18–20]. Hydrazones are an important class of compounds in clinical and medicinal chemistry with great potential for chemotherapeutic applications [21–25]. Therefore, studies on DNA binding and cytotoxic activities of copper(II)–hydrazone complexes remain as an area of interest.

In this article, we report the synthesis of two copper(II)–hydrazone complexes, $[Cu(L)(Hbpe)(ClO_4)]\cdot ClO_4\cdot[Cu(L)Cl]$ (**1**) and $[Cu(LH)_2]\cdot 1.5ClO_4\cdot 0.5OH$ (**2**), using hydrazone HL obtained by the condensation of benzhydrazide with 2-acetyl pyridine; the products were characterized by micro-analytical, FT-IR, UV–vis, EPR, cyclic voltammetric, and single-crystal X-ray diffraction methods. We also explored the DNA binding of HL and its copper complexes using UV–vis titration and viscosity measurements.

2. Experimental

2.1. *Materials*

Caution! Perchlorate salts of metals in presence of organic ligands are potentially explosive. Though we did not encounter any problem, they should be prepared in small quantity and handled with much care.

Benzhydrazide, 2-acetyl pyridine, and *trans*-1-(2-pyridyl)-2-(4-pyridyl)-ethylene (bpe) were purchased from Sigma-Aldrich Co. and used as received. $Cu(ClO_4)_2{\cdot}6H_2O$ was prepared by the treatment of basic copper carbonate, $CuCO_3{\cdot}Cu(OH)_2$ (AR grade, E. Merck, India), with 80% perchloric acid, $HClO_4$ (AR grade, E. Merck, India), followed by slow evaporation on a water bath and stored in $CaCl_2$ desiccators. The CT-DNA was purchased from Bangalore Genei; tris-buffer, sodium chloride, and hydrochloric acid (AR) were purchased from E. Merck, India. Tris(hydroxymethyl)–aminomethane–HCl (Tris–HCl) buffer was prepared using deionized and sonicated triple-distilled water.

2.2. *Syntheses*

2.2.1. Synthesis of (E)-N′-(1-(pyridine-2-yl)ethylidene)benzohydrazide (HL). The Schiff base HL was synthesized by the condensation of benzhydrazide (0.686 g, 5 mM) and 2-acetyl pyridine (0.606 g, 5 mM) in methanol (50 mL) following literature procedure [26] (scheme 1). Yield: 0.94 g (73%). Anal. Calcd for $C_{14}H_{13}N_3O$ (FW: 239.27) (%): C, 70.34; H, 5.52; N, 17.61. Found: C, 70.28; H, 5.48; N, 17.56. Main FT-IR bands (KBr, cm^{-1}): 1659 (C=N), 3178–3007 (N–H), 620, 407 (Py str.). UV–vis bands (λ/nm): 222 (br.) and 292(s).

2.2.2. Synthesis of 1. Compound **1** was synthesized on treatment of 20 mL methanolic solution of $Cu(ClO_4)_2{\cdot}6H_2O$ (0.370 g, 1 mM) and HL (2.4 mL, 1 mM) with *trans*-1-(2-pyridyl)-2-(4-pyridyl)-ethylene (0.091 g, 0.5 mM). The resulting dark green solution was stirred for 15 min at room temperature and filtered. Green needle crystals of **1** were obtained by slow evaporation of the solvent for eight days (scheme 1). Yield: 0.87 g (85%). Anal. Calcd for $C_{40}H_{35}Cl_{2.99}Cu_2N_8O_{10}$ (FW: 1020.85) (%): C, 47.06; H, 3.46; N, 10.98; Cu, 12.45. Found: C, 47.03; H, 3.42; N, 10.95; Cu, 12.40. IR bands (KBr, cm^{-1}): 1602 (C=N), 1089–1114 (ClO_4^-), 636, 456 (Py str.). UV–vis bands (λ/nm): 263 and 356 [ligand-to-metal charge transfer (LMCT)], 643 (d–d). ESI-MS: *m/z* $[Cu(L)(4'\text{-}2'\text{-Hbpe})\text{-}H]^+$: 483.1120. Found: 483.1369. $[CuL]^+$: 301.0276. Found: 301.0334.

2.2.3. Synthesis of 2. To a methanolic solution (25 mL) of $Cu(ClO_4)_2{\cdot}6H_2O$ (0.370 g, 1 mM), a methanolic solution HL (2.4 mL, 1 mM) was added. The mixture was stirred for 30 min at room temperature and filtered. Prism-shaped green crystals of **2** were obtained by slow evaporation of the solvent for five days (scheme 1). Yield: 0.51 g (73%). Anal. Calcd for $C_{28}H_{26.50}Cl_{1.50}CuN_6O_{8.50}$ (FW: 699.77) (%): C, 48.06; H, 3.82; N, 12.01; Cu, 9.08. Found: C, 48.01; H, 3.79; N, 12.00; Cu, 9.05. IR bands (KBr, cm^{-1}): 1602 (C=N), 1089–1114 (ClO_4^-), 686, 413 (Py str.). UV–vis bands (λ/nm): 255 and 360 (LMCT), 673 (d–d). ESI-MS: *m/z* Calcd for $[(HL)_2Cu]^{+2}$–H^+: 540.1335. Found: 540.1666.

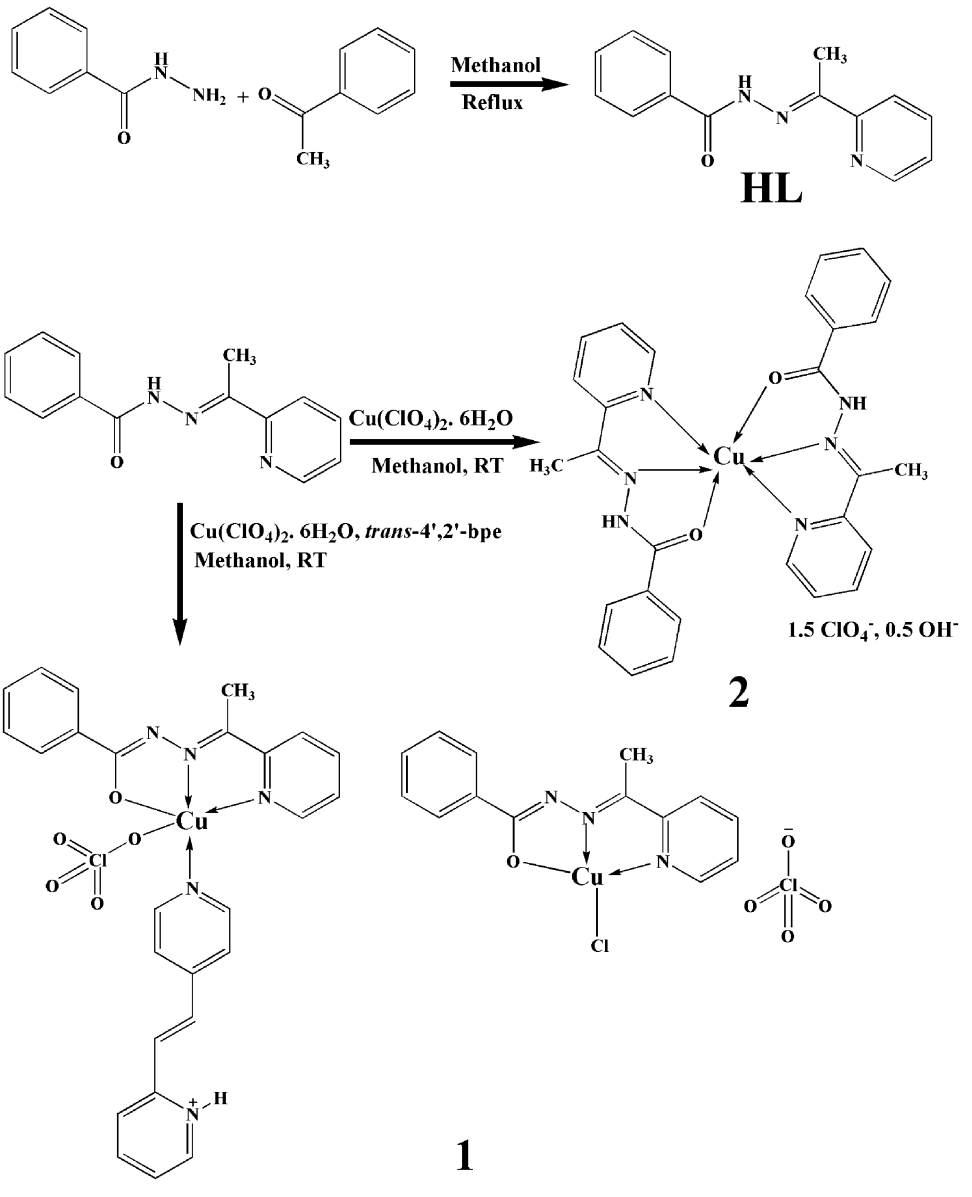

Scheme 1. Synthetic route of HL, **1**, and **2**.

2.3. *Physical measurements*

Elemental analyses were carried out using a Perkin-Elmer 2400 II elemental analyzer. The infrared spectra were recorded (4000–400 cm^{-1}) on a Perkin-Elmer RX I FT-IR spectrophotometer with KBr disks. The copper content in the complexes was estimated by standard iodometric method. The positive ion ESI-MS of **1** and **2** were performed in a QTOF micromass spectrometer using water. Electronic spectra were recorded on a Perkin-Elmer Lambda 40 UV–vis spectrophotometer using spectroscopic grade methanol or in 5 mM tris-50 mM

NaCl buffer (pH ~7.5). Concentration of DNA was determined using standard protocol as described [27]. Electrochemical measurements were performed using a PAR VersaStat-potentiostat/Galvanostat II electrochemical analysis system under dry argon using conventional three-electrode configurations in acetonitrile/tris buffer medium (pH ~7.2) with tetrabutylammonium perchlorate/KCl as the supporting electrolyte. Platinized platinum millielectrode and saturated calomel electrode (SCE) were used as working and reference electrodes, respectively, along with a platinum counter electrode. EPR spectra were measured using a Jeol JES-FA 200 ESR spectrometer for solid samples at room temperature. Viscosity measurements were conducted on an Ubbelohde viscometer, immersed in a thermostated water bath maintained at 298 K. The relative viscosities (η) of the samples were determined using the equation $\eta = (t - t_0)/t_0$, where t_0 is the flow time for buffer alone and t is the flow time of either only DNA solution or DNA solution, with different concentrations of **1** and **2**.

2.4. *X-ray crystallography*

Diffraction quality green needle crystal of **1** and green prism of **2** were mounted on a Bruker SMART CCD and on an Oxford Diffraction Xcalibur 3/CCD diffractometer, respectively, equipped with graphite mono-chromated Mo Kα radiation (λ = 0.71073 Å) from a fine-focus sealed tube radiation source. Intensity data for **1** and **2** were collected at 100 and 140 K, respectively, using thin-slice φ and ω scans. No significant intensity variation was observed during data collection. Data reductions for **1** and **2** were made by using SAINT [28] and CrysAlis and RED [29], respectively. Empirical multiscan absorption corrections were applied to the intensity values of **1** and **2** (T_{max}/T_{min} = 0.8814/0.7332 and 1.062/0.968, respectively) using SADABS [30]. The structures were solved by direct methods using SHELXS-97 [31] and refined with full-matrix least-squares based on F^2 using the SHELXL-97 [31] program. All non-hydrogen atoms were refined anisotropically. Hydrogens in **1** were located in a difference Fourier map and refined isotropically. In **2**, all hydrogens were first located in the difference Fourier map, but positioned geometrically and set to ride on their respective parent. The molecular graphics and crystallographic illustrations for **1** and **2** were prepared using Bruker SHELXTL [32], ORTEP [33], and WinGX [34] programs. Relevant crystallographic data and structure refinement parameters for **1** and **2** are summarized in table 1.

3. Results and discussion

3.1. *FT-IR spectra*

IR spectra of **1** and **2** were analyzed in comparison to that of HL, recorded from 4000 to 400 cm^{-1} (ESI: figures S1–S3, see online supplemental material at http://dx.doi.org/10.1080/00958972.2014.964697). In the ligand, stretching vibrations for –NH and –C=N groups were observed at 3178–3007 and 1659 cm^{-1} [22, 23, 35, 36], respectively. The imine (–C=N) stretch of HL shifted to lower wavenumbers in spectra of **1** and **2** at 1602 cm^{-1}, suggesting its coordination to metal and also attributed to delocalization of the lone pair [5, 6, 35, 36]. Typical trifurcated bands for perchlorate at 1089–1114 cm^{-1} indicated its presence in the complexes [5, 6, 35, 36]. Low-energy in-plane and out-of-plane pyridine ring vibrations were shifted to higher frequencies in **1** (636 and 456 cm^{-1}) and **2** (686 and 413 cm^{-1}) compared to that of HL (620 and 407 cm^{-1}), which may be attributable to the rigidity due to complexation [22, 23, 35, 36].

Table 1. Crystallographic and refinement data for **1** and **2**.

Complexes	**1**	**2**
Empirical formula	$C_{40}H_{35}Cl_3Cu_2N_8O_{10}$	$C_{28}H_{26.5}Cu\ N_6\ O_{8.5}Cl_{1.5}$
Formula weight (g M^{-1})	1020.85	699.77
Crystal system	Monoclinic	Triclinic
Space group	$P2_1/c$	$P\text{-}1$
Z	4	2
a (Å)	11.7153(9)	9.9647(7)
b (Å)	13.3843(14)	11.6858(8)
c (Å)	26.396(3)	13.6336(10)
α (°)	90	103.607(6)
β (°)	94.755(5)	103.607(6)
γ (°)	90	92.602(6)
V (Å^3)	4124.7(7)	1491.15(18)
Temperature (K)	100(2)	140(1)
Density (Mg m^{-3})	1.644	1.559
Absorption coefficient (mm^{-1})	1.295	0.929
F (0 0 0)	2080	718
Crystal dimension (mm)	0.42 × 0.20 × 0.10	0.46 × 0.07 × 0.04
θ Range for data collection (°)	1.55–27.48	3.5–21.25
Reflections collected	41,784	12,454
Independent reflections (R_{int})	9369 (0.0884)	3278 (0.158)
"Observed" reflections	5868	1879
Goodness-of-fit, F^2	1.001	0.930
R indices (all data)	$R_1 = 0.099$, $wR_2 = 0.100$	$R_1 = 0.130$, $wR_2 = 0.125$
Final R indices [$I > 2\sigma(I)$]	$R_1 = 0.046$, $wR_2 = 0.084$	$R_1 = 0.063$, $wR_2 = 0.108$
Largest diff. peak and hole (e Å^{-3})	0.48 and −0.57	0.72 and −0.38

3.2. *UV–vis spectra*

UV–vis spectra of HL and its complexes were recorded at room temperature in methanol (ESI: figures S4–S6). The electronic spectra of **1** and **2** are in good agreement with their geometries. The spectra of HL exhibited two charge transfer (CT) bands at 292 and 222 corresponding to $n \rightarrow \pi^*$ and $\pi \rightarrow \pi^*$ transitions. Ligand-centered CT band at 222 nm undergoes large bathochromic shift at 256 and 263 nm in spectra of **1** and **2**, respectively. New absorptions corresponding to LMCT appeared at 356 and 360 nm for **1** and **2**, respectively. A weak and broad band corresponding to d–d transition of the metal ion appeared at 643 and 673 nm in **1** and **2**, which are in very good agreement with their square-pyramidal and octahedral geometries, respectively [22, 23, 37].

3.3. *Crystal structures and EPR spectra of 1 and 2*

3.3.1. Crystal structure of 1. An ORTEP view of **1** with atom numbering scheme is shown in figure 1 and the bonding parameters are presented in table 2. Compound **1** consists of $[Cu(L)(Hbpe)ClO_4]^+$, a perchlorate, and a neutral complex [Cu(L)Cl]. Within the cationic unit, the copper(II) is coordinated by an anionic Schiff base ligand, L^-, a protonated bpe ligand (Hbpe), and a perchlorate. L^- is coordinated in tridentate fashion through its pyridine nitrogen (N1), imine nitrogen (N8), and *enolato* oxygen (O17). Hbpe coordinated to the Cu1 through 4-pyridyl nitrogen (N20); its 2-pyridyl nitrogen (N29) is protonated. The coordinated perchlorate is attached to the metal *via* O12. Thus, geometry around Cu1 can be best described by distorted square-pyramidal geometry which is satisfied by N_3O_2 donor set.

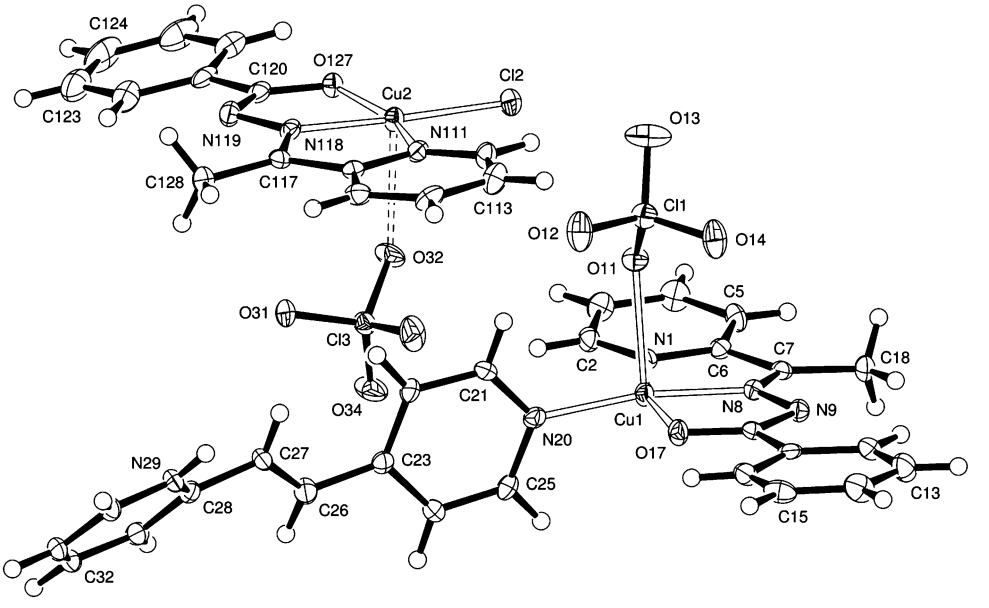

Figure 1. ORTEP view of **1**, indicating the atom labeling scheme. Displacement ellipsoids are at the 50% probability level.

The other perchlorate present in the complex unit neutralizes the charge of the cationic unit. Cu–$O_{(perchlorate)}$ bond length (Cu1–$O11_{(perchlorate)}$ 2.432(2) Å) is quite long compared with the other Cu–O bond (Cu1–$O17_{(enolato)}$ 1.957(2) Å) length in the cationic unit. The distorted square-pyramidal geometry around copper(II) is evident from the bonding parameters (table 2) and also supported by the Addison parameter [38], τ, which has a value of 0.161 for Cu1. The slightly elongated Cu1–N20 length could be attributed to the delocalization of the positive charge on N29 throughout the bpe^+ skeleton (table 2). The Cu2 of [Cu(L)Cl] is coordinated with a L^- in the same fashion as in the cationic unit, and also coordinated with a chloride generated *in situ*. Thus, the four-coordinate geometry of Cu2 is described as distorted square planar with the N_2OCl donor set (figure 1). The C10–O17 and C120–O127 bond lengths, respectively, in the cationic and the neutral units of **1** are comparable with the *enolato* C–O bond lengths found in complexes reported earlier [5, 39], thus indicating that carbonyl functionality coordinates in *enolic* form in **1**.

In **1**, Cu2 coordinated with chloride though no chloride source was used during the course of reaction. This Cl^- may be generated *in situ* from ClO_4^- either during the preparation of $Cu(ClO_4)_2{\cdot}6H_2O$ in strong $HClO_4$ medium or during the synthesis of **1**. Here, Cl^- ion is preferred over ClO_4^- ion to coordinate in the fourth coordination site of Cu2 possibly due to steric effects, while its complementary H_3O^+ ion protonates the uncoordinated N29 end of the *trans*-bpe ligand attached to the Cu1. In turn, this N–bound H atom makes a short intermolecular hydrogen bond of 1.85 A to O127 bound to Cu2.

3.3.2. Crystal structure of 2. An ORTEP view of **2** with atom numbering scheme is shown in figure 2 and selected bond dimensions are given in table 2. **2** is a mono-nuclear cationic unit in which the central copper(II) is coordinated by two tridentate HL ligands,

Table 2. Selected bond lengths (Å) and angles (°) for **1** and **2**.

1			
Cu1–O11	2.432(2)	Cu2–O127	2.006(2)
Cu1–O17	1.957(2)	Cu2–N111	1.993(3)
Cu1–N1	2.031(3)	Cu2–N118	1.935(3)
Cu1–N8	1.924(3)	Cu2–Cl2	2.2122(9)
Cu1–N20	1.972(3)	C120–O127	1.313(4)
C10–O17	1.298(4)	–	–
O11–Cu1–O17	98.12(9)	O127–Cu2–N111	159.39(10)
O11–Cu1–N1	85.86(9)	O127–Cu2–N118	78.99(10)
O11–Cu1–N8	93.17(10)	N111–Cu2–N118	80.65(11)
O11–Cu1–N20	96.14(9)	Cl2–Cu2–N111	101.47(8)
O17–Cu1–N1	160.78(10)	Cl2–Cu2–N118	177.25(8)
O17–Cu1–N20	96.18(10)	Cl2–Cu2–O127	98.78(7)
O17–Cu1–N8	80.41(10)		
N1–Cu1–N20	102.11(10)		
N1–Cu1–N8	80.59(10)		
N8–Cu1–N20	170.47(11)		
2			
Cu–O1	2.033(5)	Cu–N42	2.033(7)
Cu–O5	2.388(5)	Cu–N82	2.255(7)
Cu–N3	1.907(6)	C1–O1	1.267(10)
Cu–N7	2.018(6)	C5–O5	1.237(10)
O1–Cu–O5	85.47(19)	O5–Cu–N82	147.8(2)
O1–Cu–N3	79.0(3)	N3–Cu–N7	178.3(3)
O1–Cu–N7	99.4(2)	N3–Cu–N42	79.4(3)
O1–Cu–N42	157.7(2)	N3–Cu–N82	106.1(3)
O1–Cu–N82	97.5(2)	N7–Cu–N42	102.1(3)
O5–Cu–N3	105.9(2)	N7–Cu–N82	74.7(3)
O5–Cu–N7	73.2(2)	N42–Cu–N82	93.7(3)
O5–Cu–N42	95.2(2)	–	–

each *mer*, with a distorted octahedral geometry. Coordination sphere around copper is satisfied by pyridyl nitrogen atoms (N42 and N82), imino nitrogens (N3 and N7), and keto oxygens (O1 and O5) from two different neutral ligands. The C1–O1 and C5–O5 bond lengths are much shorter than expected *enolato* bond lengths [22, 39], and the location of hydrogens on N2 and N6 confirms the *keto* form of the coordinated ligands. The complex is thus dicationic; 1.5 perchlorate anions and 0.5 hydroxyl anions present in **2** neutralize the charges. Due to Jahn–Teller elongation of geometry around copper(II), the Cu(II)–N(imine) bonds as well as the Cu(II)–$N_{pyridyl}$ and Cu(II)–O_{keto} bonds in one ligand are significantly shorter than in the other (table 2). The Cu ion thus fits eccentrically in the cavity provided by donors in the two ligand planes. The *trans* angle, N7–Cu–N3 is close to linear, but the other *trans* angles, O5–Cu–N82 and O1–Cu–N42, governed by the ligand shape and dimensions, show marked deviations from 180°.

A rather weak N2–H2…O5′ hydrogen bond links the complex cations in dimer pairs about centers of symmetry. The other amine forms a stronger hydrogen bond to the perchlorate; thus, it is proposed, also receives a hydrogen bond from a partially occupied hydroxyl ion which also links to a half-occupied perchlorate (table 3).

Thus, when the metal salt is treated only with Schiff base, (**2**), the metal is coordinated by two Schiff base molecules in a distorted octahedral geometry, whereas in the presence of bpe, (**1**), a mixture of Cu complexes in two different geometries (distorted square-pyramidal and distorted square-planar) is observed.

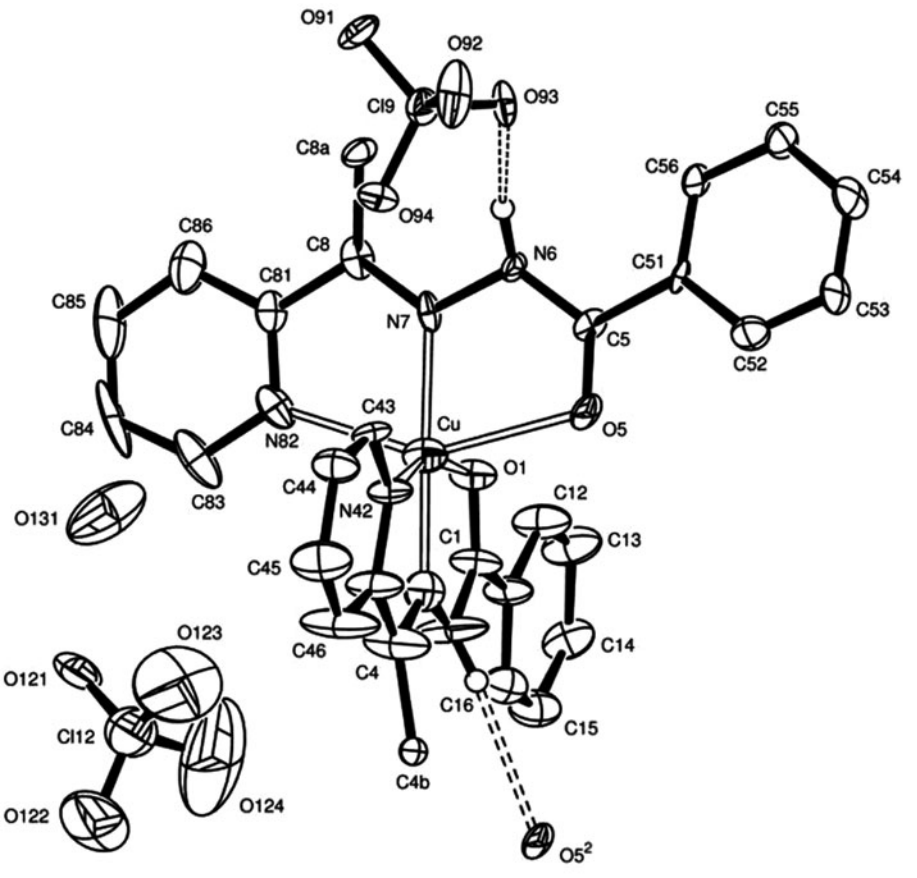

Figure 2. ORTEP view of **2**, indicating the atom labeling scheme. Hydrogens are omitted for clarity. Thermal ellipsoids are at the 50% probability level.

Table 3. Hydrogen bonding parameters (Å, °) for **2**.

	d(D–H)	*d*(H…A)	*d*(D…A)	∠D–H…A
N(2)–H(2)…O(5′)	0.81(7)	2.42(7)	3.202(9)	165(8)
N(6)–H(6)…O(93)	0.92(6)	2.00(6)	2.875(8)	159(6)

3.3.3. EPR spectra of 1 and 2. To obtain further information about the stereochemistry, site of metal–ligand bonding and spin states of metal ions, X-band EPR spectra of the complexes were recorded in powder state at room temperature using 9.5 GHz field modulation. For **1**, EPR signal (figure 3) exhibits a characteristic line shape for powder sample containing a paramagnetic ion without any hyperfine splitting. Due to dipolar–dipolar interaction, the spectrum shows only one broad line $g_{iso} = 2.055$ [40]. Analysis of **2** (figure 4) gives $g_{\|} = 2.117$, $g_{\perp} = 2.054$. The trend $g_{\|} > g_{\perp} > 2.0023$ observed for **2** indicates a distorted tetragonal geometry and the unpaired electron is localized in the $d_{x^2-y^2}$ orbital of the copper(II) ion [41].

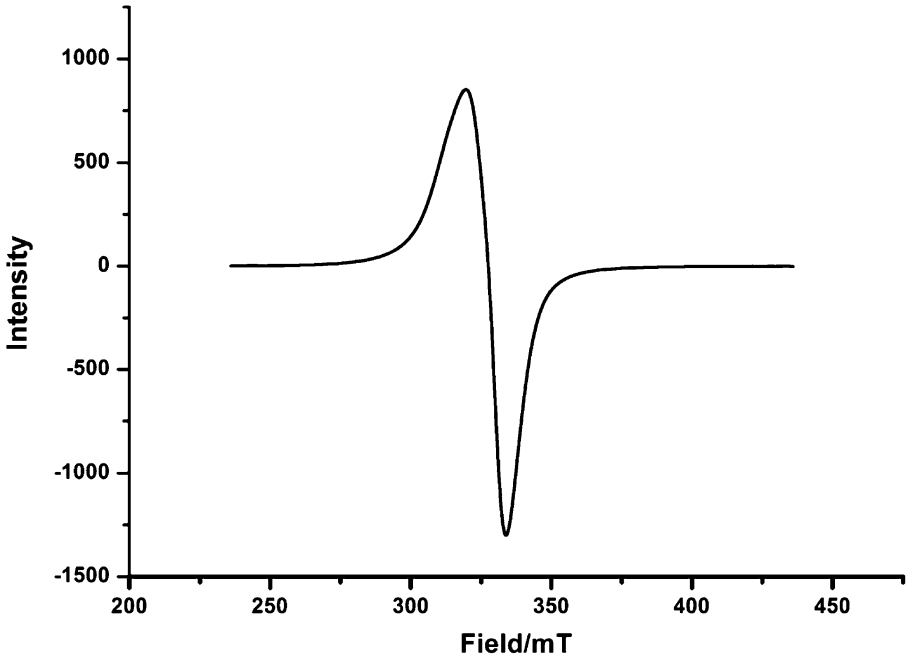

Figure 3. Powder X-band EPR spectrum of **1** recorded at room temperature.

3.4. *DNA binding study*

3.4.1. Electronic absorption titration. The stability of HL, **1,** and **2** in buffer solution at room temperature was monitored by UV–vis spectroscopy for 24 h. There was no change in the spectral features, revealing the compounds are stable under these conditions. Positive ion electrospray mass spectra of the complexes in water give the molecular ion peaks at *m/z* 483.1369 and 301.0334 for **1** (ESI: figure S7) and at *m/z* 540.1335 for **2** (ESI: figure S8). The signal for **1** corresponds to $[Cu(L)(4'\text{-}2'\text{-}Hbpe)\text{-}H]^+$ and $[Cu(L)]^+$, whereas the signal for **2** at *m/z* 540.1666 can be attributed to $[Cu(HL)_2\text{-}H]$. These data also supported the stabilities of both **1** and **2** in solution.

HL had a band at 292 nm, as mentioned earlier, showed hypochromism with addition of increasing amounts of DNA solution [0–50 μM]. An isosbestic point also appeared in the UV–vis titration spectra of HL at 277 nm indicating the presence of two absorbing species in solution (figure 5). For **1**, the CT bands were observed in tris-buffer at 263 and 356 nm. In this case, upon addition of increasing amounts of DNA [0–50 μM], the former bands underwent hypochromism and later experienced hyperchromism; for ease of data handling, the change of intensity of the band at 356 nm was taken into account. For the titration experiment of **1** with CT-DNA, in addition to hyperchromism, an isosbestic point appeared at 320 nm during the titration. Addition of CT-DNA results in a hyperchromism in absorption intensity, indicating that there exists an interaction between **1** and CT-DNA, which is different from classical intercalation. These spectral features are analogous to that of previously reported complexes [42, 43], whose interaction mode with DNA is groove binding. The observations of these spectral studies suggested that **1** may bind to CT-DNA, possibly

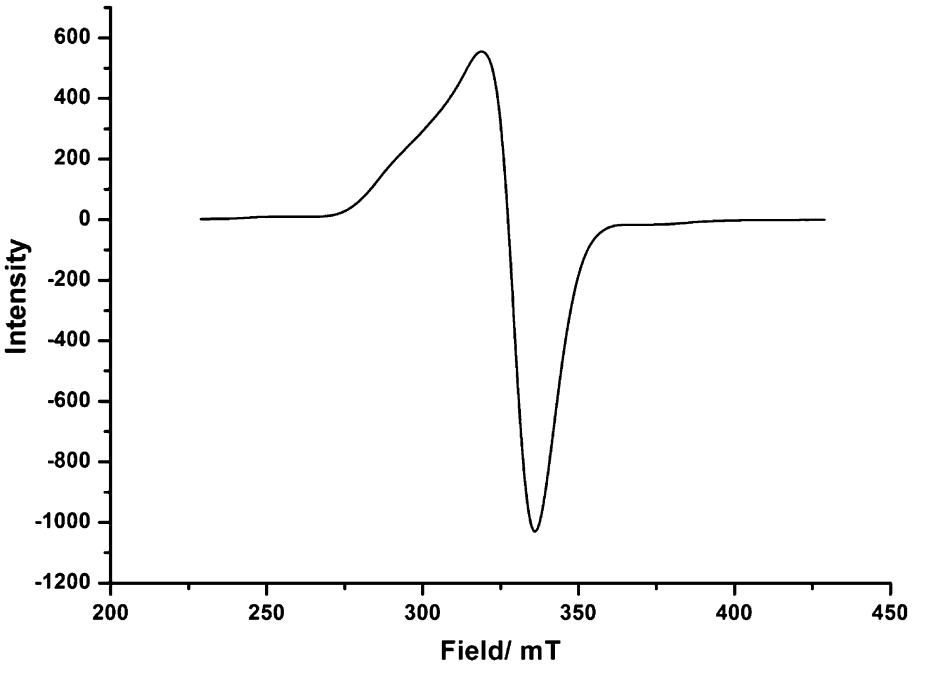

Figure 4. Powder X-band EPR spectrum of **2** recorded at room temperature.

via groove binding. The change in spectral pattern of **1** upon addition of DNA [0–50 μM] is depicted in figure 6. Complex **2** showed CT bands in tris-buffer medium at 255 and 360 nm. Upon addition of increasing aliquot [0–50 μM] of CT-DNA to a solution, the band at 255 nm showed considerable hyperchromism, whereas the band at 360 nm did not show any significant effect (figure 7). As CT-DNA itself absorbs at this region of wavelength, a blank titration was performed and the absorbance data for DNA titration of **2** were corrected with these data. The band at 255 nm did not shift ($\Delta\lambda$ ~4 nm) much and also provided evidence for presence of groove-binding interaction between CT-DNA and **2**, like **1** [42–44]. By regression analysis using equation (1) [45], the binding constants (K) of **1** and **2** with DNA were calculated,

$$1/\Delta A = 1/\Delta A_{\max} + 1/K\Delta A_{\max} \times 1/(C_{\mathrm{D}} - C_{\mathrm{O}}) \quad (1)$$

where ΔA is the change in absorbance at 292 nm for HL, 356 nm for **1,** and 255 nm for **2**, and $\Delta A_{\max}$ is the same parameter when the respective species are totally bound to CT-DNA. C_{D} is the concentration of CT-DNA and C_{O} is the initial concentration of each compound being used. The double-reciprocal plots (figure 8) were used for the determination of the binding constant (K) using equation (1), which yielded the K values to be 9.5×10^3, 1.88×10^4, and 4.66×10^4 M^{-1} for HL, **1**, and **2**, respectively. The binding constant data indicate clearly that upon coordination with copper(II), the DNA binding ability of HL is enhanced. The DNA binding constants of HL, **1**, and **2**, follow the order $K_2 > K_1 > K_{\mathrm{HL}}$. HL is a neutral species. Complex **2** contains $a + 2$ charge which is mainly localized upon copper(II), whereas **1** (cationic part) contains $a + 1$ charge due to protonation of the

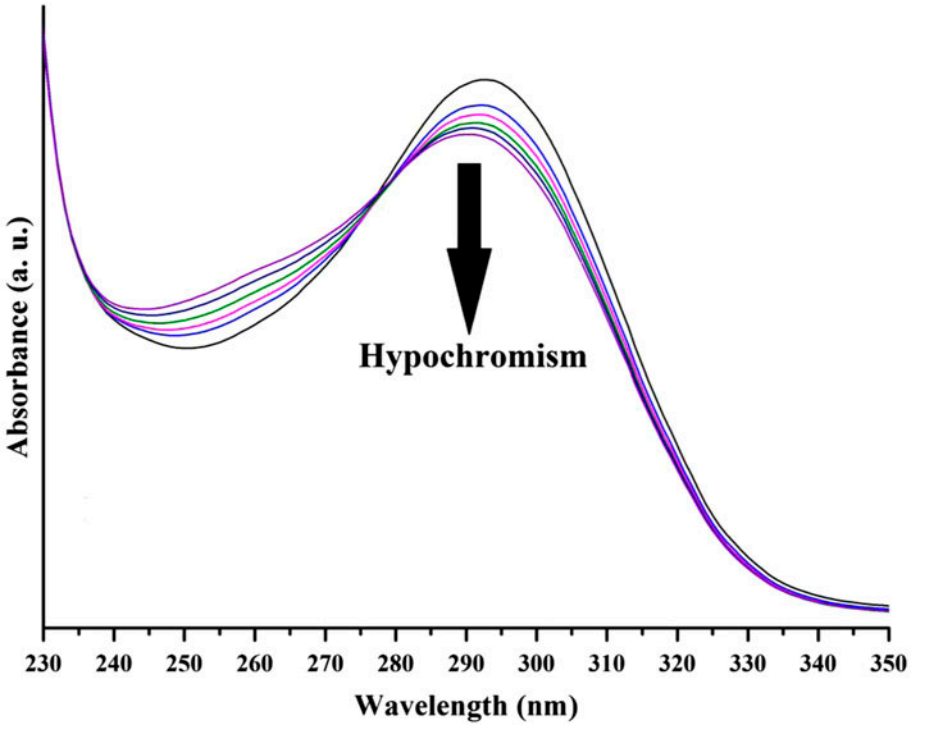

Figure 5. The change in absorbance of HL upon addition of increasing concentration of CT-DNA (0–50 μM) in 5 mM Tris-50 mM NaCl at pH 7.

trans-bpe fragment, and this charge is delocalized over the highly conjugated *trans*-bpe ligand. Thus, the effective nuclear charge of **2** is much higher than that of **1** and hence, **2** shows greater DNA binding ability than **1**.

In spite of the different complex species and coordination environment, the DNA binding abilities of **1** and **2** may be compared to the copper complexes reported earlier [13, 14, 18–21, 42, 43, 47–51] in terms of binding mode and binding constant K_b with CT-DNA. Most of the complexes can bind with DNA through intercalation between DNA base pairs [13, 14, 18–21, 47–51] by means of strong $\pi\cdots\pi$ stacking interaction, whether a few can bind at major or minor grooves of DNA [42, 43] through strong hydrogen bonds or electrostatic interactions. Binding capability comparison between the investigated complexes and compounds reported herein revealed that they show lower binding abilities compared to the classical intercalator [46] and some discussed complexes, but higher abilities in comparison to some mono- and bi-nuclear copper(II) complexes [20, 47].

3.4.2. Voltammetric study of DNA-complex interaction. Cyclic-voltammetric studies are also very efficient tools to elucidate the nature of binding between DNA and metal complexes [52]. The cyclic voltammetric studies of **1** and **2** in the absence and presence of CT-DNA were performed in tris-buffer (pH ~7.2) at room temperature under dry nitrogen atmosphere (figures 9 and 10). Complexes **1** and **2** in the buffer medium showed an irreversible reduction at −0.48 and −0.49 (*vs.* SCE), respectively. For both cases, no oxidation

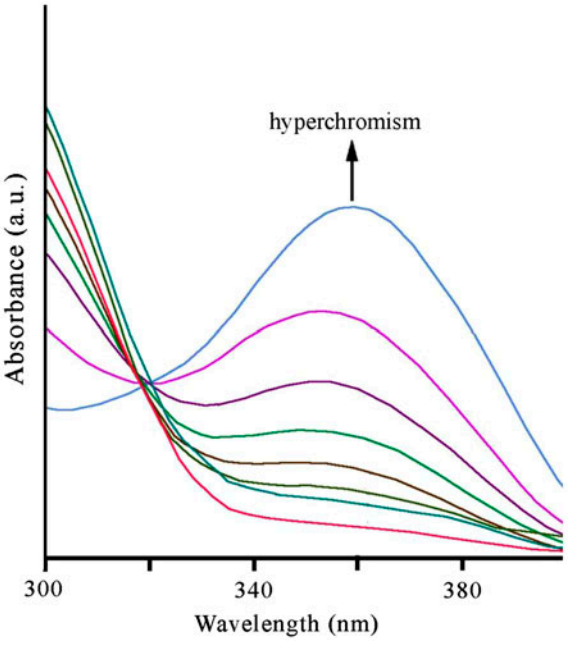

Figure 6. The change in absorbance of **1** upon addition of increasing concentration of CT-DNA (0–50 μM) in 5 mM Tris-50 mM NaCl at pH 7.

peaks are observed. On comparing with previously reported mono-nuclear Cu(II) systems [53, 54], the reductions were assigned to Cu(II)–Cu(I) reduction. In case of **1**, gradual addition of CT-DNA to the complex solution leads to increase in peak current. During binding of **1** with DNA, electro-active Cu(II) center may become more exposed to electrode surface, and hence steadily enhanced the peak current [55]. For **2**, reduction peaks decreased obviously with a positive shift (+2 mV), which further proved a groove binding mode between the two species [56].

3.4.3. Viscosity measurement. When small molecules intercalate between DNA base pairs, they give an increase in viscosity of a solution of DNA, whereas non-classical interactive binding leads to lowering of the viscosity with surface or groove binding of small molecules with DNA; the viscosity of the solution does not change [57–59]. In the present case, the relative viscosity (η/η_0) of the DNA solutions showed almost no change with addition of increasing concentration of **1** (figure 11: green line) and **2** (figure 11: red line), which concluded beyond doubt that **1** and **2** bind with DNA via surface or groove binding.

3.5. *Electrochemistry*

Electrochemical properties of the complexes were studied at room temperature using HPLC-grade acetonitrile using tetrabutylammonium perchlorate as supporting electrolyte at a scan rate of 50 mVs^{-1} from +2.0 to −2.0 V. In the voltammogram of **1** (figure 12), on

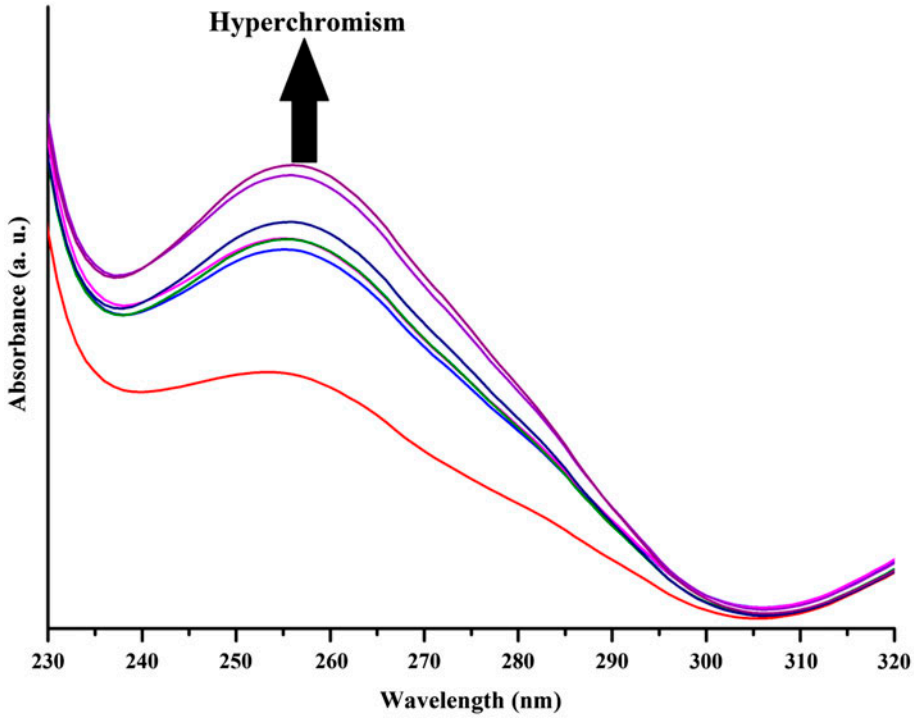

Figure 7. The change in absorbance of **2** upon addition of increasing concentration of CT-DNA (0–50 μM) in 5 mM Tris-50 mM NaCl at pH 7.5.

cathodic scan, several reductive responses were observed at –1.34, –0.98, –0.66, and –0.45 V (*vs.* SCE). Higher peaks, –1.34 and –0.98 V, may be attributed to the reduction of –N=N– or –C=N– moieties present in the coordinated ligands. Other cathodic responses (–0.66 and –0.45 V) are conveyable to two Cu(II)/Cu(I) reductions corresponding to two independent copper(II) ions associated with different geometrical environments present in **1**. The former reduction peak can be attributed from Cu(II) to Cu(I) reduction in [Cu(L)Cl], while the latter can be for cationic $[Cu(L)(Hbpe)ClO_4]^+$. On reverse scan, corresponding oxidative responses (Cu(I)/Cu(II) oxidation) were observed at –0.87 and –0.07 V (*vs.* SCE), respectively. Thus peak-to-peak separations of 210 and 380 mV indicate the irreversible nature of these redox processes. On changing the scan rate, redox responses slightly shifted to more anodic values, while I_{pc} remain greater than I_{pa} and peak-to-peak separations always remain greater than 50 mV that confirm the irreversible nature of these redox processes. A peak with narrow width and large peak current is observed during anodic scan, which can be assigned to the oxidation of the surface adsorbed metallic copper [60].

Voltammogram of **2** (figure 13) reveals that on cathodic scan, **2** displayed an irreversible reductive response at –0.75 V (*vs.* SCE) assignable to Cu(II)/Cu(I) reduction. Similar to **1**, on reverse scan, a peak at –0.19 V (*vs.* SCE) associated with narrow width and large peak current corresponds to the anodic oxidation of the surface-adsorbed metallic copper [61].

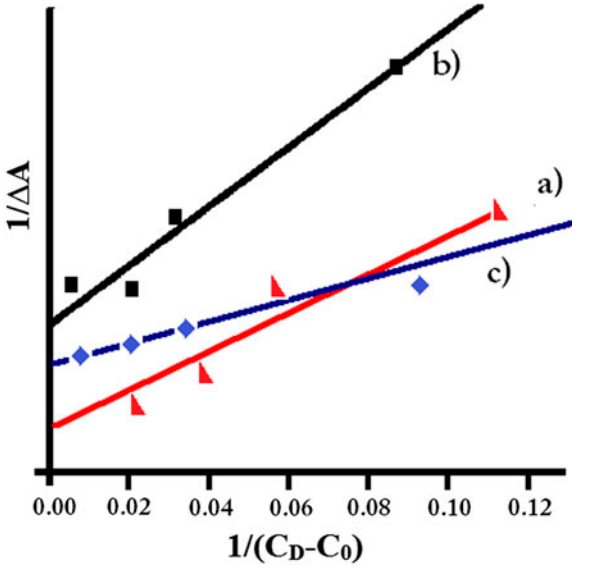

Figure 8. Plot of $1/\Delta A$ *vs.* $1/C_D - C_O$ (a) for HL, (b) for **1**, and (c) for **2**.

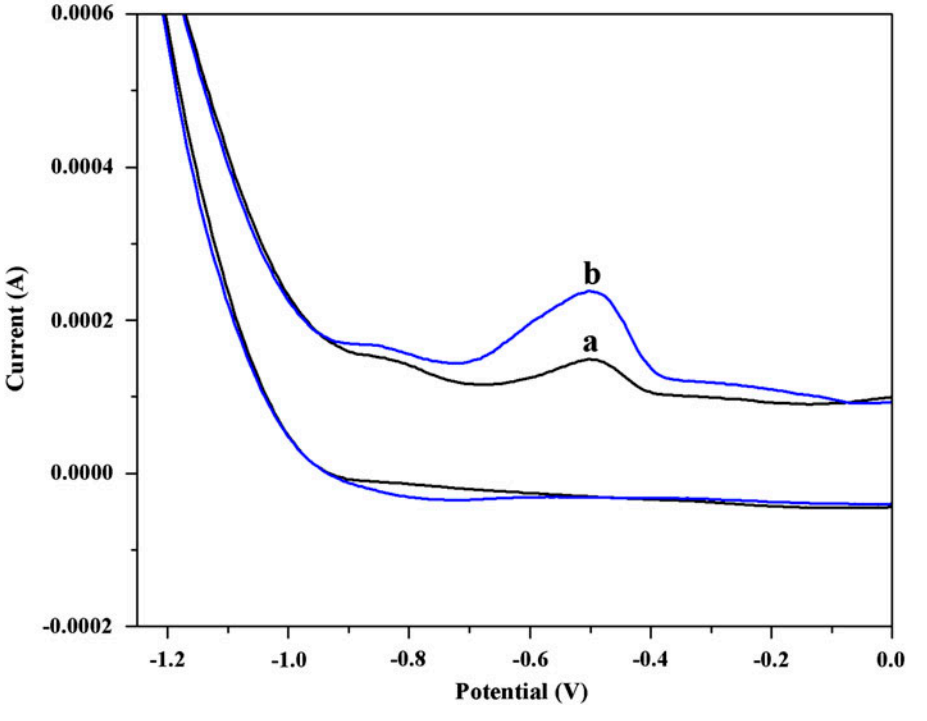

Figure 9. Cyclic voltammograms of **1** in 5 mM Tris-50 mM NaCl at pH 7, (a) in the absence and (b) in the presence of CT-DNA.

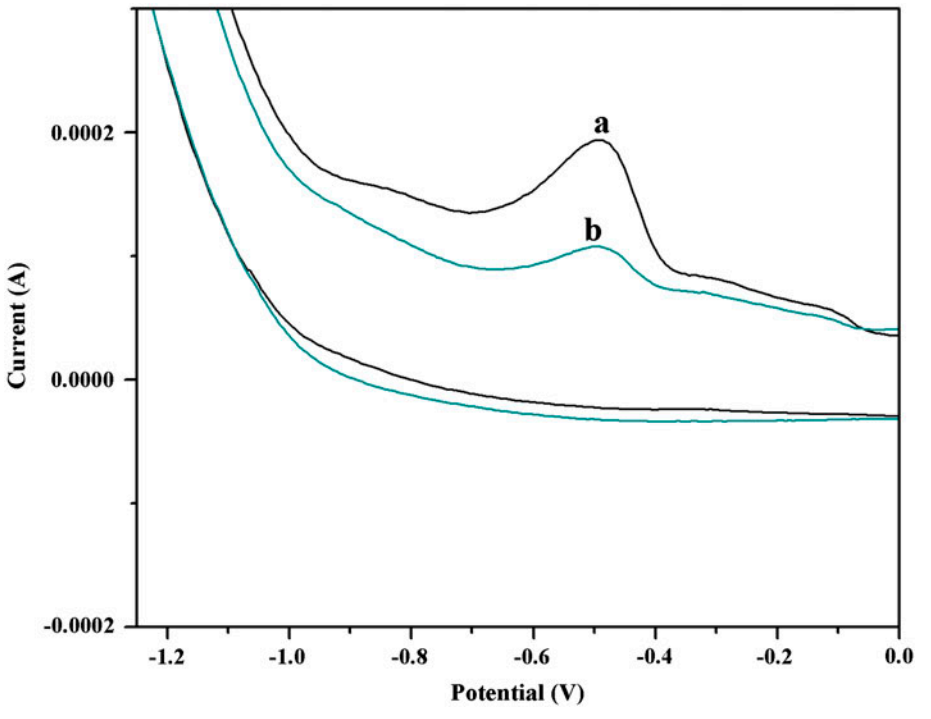

Figure 10. Cyclic voltammograms of **2** in 5 mM Tris-50 mM NaCl at pH 7, (a) in the absence and (b) in the presence of CT-DNA.

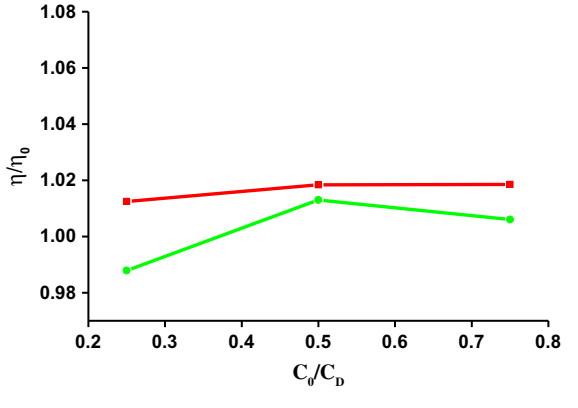

Figure 11. Plot of η/η_0 *vs.* C_O/C_D for **1** (green line) and for **2** (red line). The symbols have their usual meanings as described in the text (see http://dx.doi.org/10.1080/00958972.2014.964697 for color version).

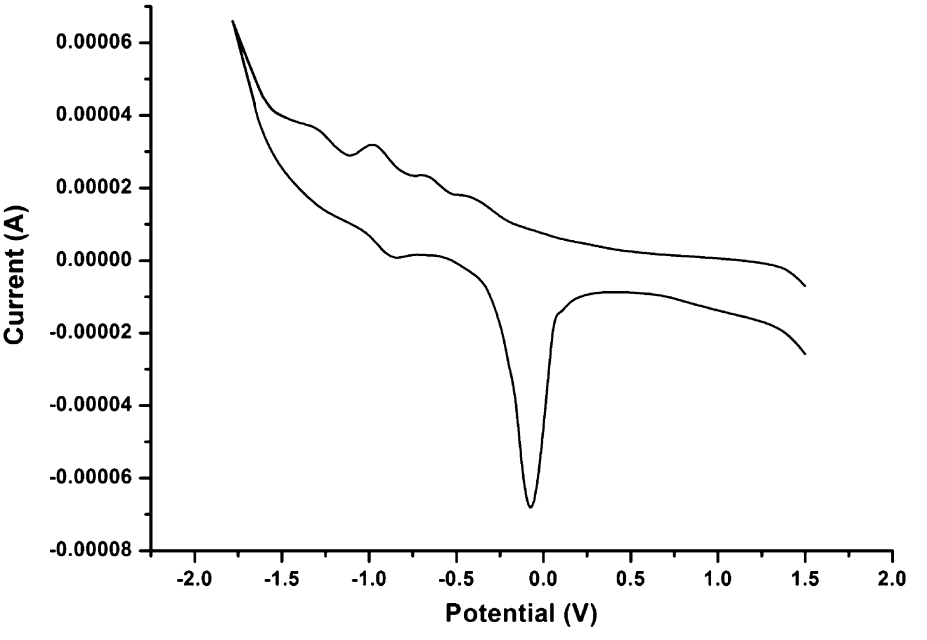

Figure 12. The cyclic voltammogram of **1** recorded at room temperature in acetonitrile.

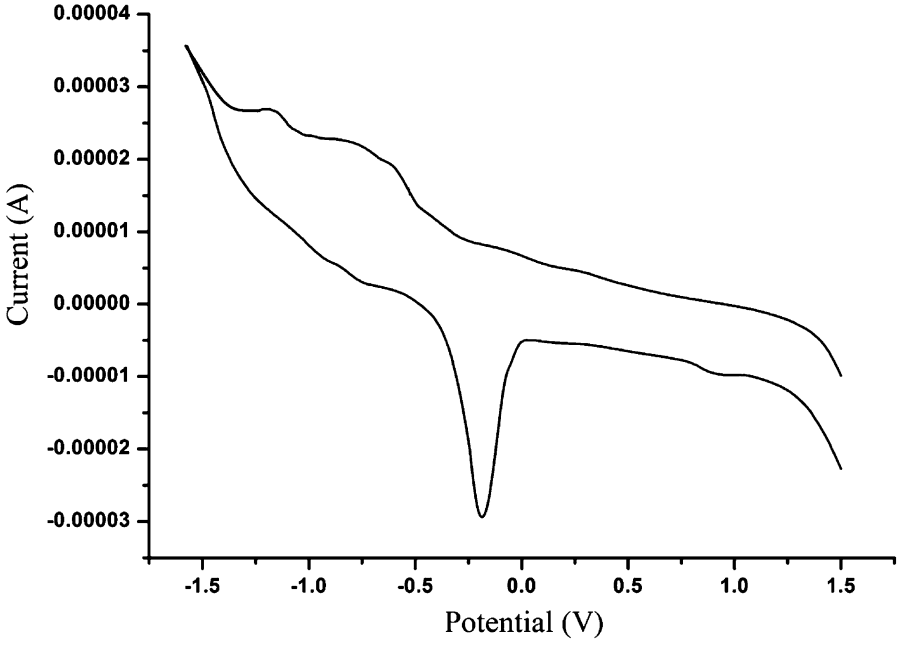

Figure 13. The cyclic voltammogram of **2** recorded at room temperature in acetonitrile.

4. Conclusion

We have reported the synthesis, spectral, and structural characterization of two new aroyl hydrazone derived copper(II) complexes. Structural characterization reveals that metal ion is octahedral with only the Schiff base, whilst two distinct metal center geometries are adopted; distorted square-pyramidal and distorted square-planar in the presence of both Schiff base and 4′, 2′-bpe, which indicates that the second ligand plays an important structure determining role. DNA binding abilities of complexes were tested; compared to the free ligand, the results show a significantly improved interaction for the complexes (~2 fold in **2** and ~5 fold in **1**) with respect to HL. This fact, attributed to the presence of di- and monocationic species in **2** and **1**, respectively, confirms that species with a more positive charge show stronger binding ability with electron-rich DNA helices. Viscosity measurements also suggest a surface or groove binding mode of interaction between CT-DNA and the ligand in its copper(II) complexes.

Supplementary material

CCDC 687763 and CCDC 703303 contain the supplementary crystallographic data for **1** and **2** reported in this article. These data can be obtained free of charge from the Cambridge Crystallographic Data Center via www.ccdc.cam.ac.uk/data_request/cif.

Acknowledgements

M. Nandy gratefully acknowledges the Council of Scientific and Industrial Research (CSIR), New Delhi, Government of India, for awarding Senior Research Fellowship (SRF) to him [CSIR Sanction No. 09/096(0598)/2009–EMR–I]. Thanks are also extended to the University Grants Commission, New Delhi, for financial assistance to Dr. S. Mitra as emeritus fellow [F.6-6/EMERITUS-2013-14-GEN-2214/(SA-II)] to carry out this work. Thanks are also extended to Dr. S. Das, Assistant Professor, Department of Chemistry, J.U., for the helpful discussion about DNA interaction studies.

References

[1] A.K. Patra, S. Dhar, M. Nethaji, A.R. Chakravarty. *Dalton Trans.*, 896 (2005).
[2] S. Mathur, S. Tabassum. *Chem. Biodivers.*, **3**, 312 (2006).
[3] S.E. Wolkenberg, D.L. Boger. *Chem. Rev.*, **102**, 2477 (2002).
[4] A.E. Friedman, C.V. Kumar, N.J. Turro, J.K. Barton. *Nucleic Acids Res.*, **19**, 2595 (1991).
[5] A.M. Pyle, T. Morii, J.K. Barton. *J. Am. Chem. Soc.*, **112**, 9432 (1990).
[6] C.-H. Ng, W.-S. Wang, K.-V. Chong, Y.-F. Win, K.-E. Neo, H.-B. Lee, S.-L. San, R.N.Z.R.A. Rahman, W.K. Leong. *Dalton Trans.*, **42**, 10233 (2013).
[7] D.S. Raja, N.S.P. Bhuvanesh, K. Natarajan. *Dalton Trans.*, **41**, 4365 (2012).
[8] A.M. Pyle, J.P. Rehmann, R. Meshoyrer, C.V. Kumar, N.J. Turro, J.K. Barton. *J. Am. Chem. Soc.*, **111**, 3051 (1989).
[9] P. Krishnamoorthy, P. Sathyadevi, A.H. Cowley, R.R. Butorac, N. Dharmaraj. *Eur. J. Med. Chem.*, **46**, 3376 (2011).
[10] J. Cao, J.-C. Liu, W.-T. Deng, N.-Z. Jin. *CrystEngComm*, **15**, 6359 (2013).
[11] C. Santini, M. Pellei, V. Gandin, M. Porchia, F. Tisato, C. Marzano. *Chem. Rev.*, **114**, 815 (2014).
[12] K.L. Haas, K.J. Franz. *Chem. Rev.*, **109**, 4921 (2009).

[13] T.-T. Xing, S.-H. Zhan, Y.-T. Li, Z.-Y. Wu, C.-W. Yan. *J. Coord. Chem.*, **66**, 3149 (2013).
[14] X.-L. Wang, M. Jiang, Y.-T. Li, Z.-Y. Wu, C.-W. Yan. *J. Coord. Chem.*, **66**, 1985 (2013).
[15] V. Rajendiran, R. Karthik, M. Palaniandavar, H. Stoeckli-Evans, V.S. Periasamy, M.A. Akbarsha, B.S. Srinag, H. Krishnamurthy. *Inorg. Chem.*, **46**, 8208 (2007).
[16] S. Ambika, S. Arunachalam, R. Arun, K. Premkumar. *RSC Adv.*, **3**, 16456 (2013).
[17] F. Arjmand, Md. Muddassir, Y. Zaidi, D. Ray. *MedChemComm*, **4**, 394 (2013).
[18] Y. Mei, J.-J. Zhou, H. Zhou, Z.-Q. Pan. *J. Coord. Chem.*, **65**, 643 (2012).
[19] O.A. El-Gammal, G.M. Abu El-Reash, S.E. Ghazy, T. Yousef. *J. Coord. Chem.*, **65**, 1655 (2012).
[20] K. Pothiraj, T. Baskaran, N. Raman. *J. Coord. Chem.*, **65**, 2110 (2012).
[21] B. Murukan, B.S. Kumari, K. Mohanan. *J. Coord. Chem.*, **60**, 1607 (2007).
[22] S. Banerjee, S. Mondal, S. Sen, S. Das, D.L. Hughes, C. Rizzoli, C. Desplanches, C. Mandal, S. Mitra. *Dalton Trans.*, 6849 (2009).
[23] S. Banerjee, S. Mondal, W. Chakraborty, S. Sen, R. Gachhui, R.J. Butcher, A.M.Z. Slawin, C. Mandal, S. Mitra. *Polyhedron*, **28**, 2785 (2009).
[24] K. Ghosh, P. Kumar, N. Tyagi, U.P. Singh, V. Aggarwal, M.C. Baratto. *Eur. J. Med Chem.*, **45**, 3770 (2010).
[25] Y.-C. Liu, Z.-Y. Yang. *J. Biochem.*, **147**, 381 (2010).
[26] S. Sen, S. Mitra, D.L. Hughes, G. Rosair, C. Desplanches. *Inorg. Chim. Acta*, **360**, 4085 (2007).
[27] M.E. Reichmann, S.A. Rice, C.A. Thomas, P. Doty. *J. Am. Chem. Soc.*, **76**, 3047 (1954).
[28] Bruker. *SMART and SAINT. Area Detector Control and Integration Software*, Bruker Analytical X-ray Instruments Inc., Madison, WI (1997).
[29] 'CrysAlis-CCD and RED'. *Programs for Processing Xcalibur Data*, Oxford Diffraction Ltd, Abingdon (2005).
[30] G.M. Sheldrick. *SADABS, Program for Empirical X-ray Absorption Correction*, Bruker-Nonius, Madison, WI (1990–2004).
[31] G.M. Sheldrick. *Acta Cryst.*, **A64**, 112 (2008).
[32] G.M. Sheldrick. *SHELXTL (Version 5.1), Program for the Solution and Refinement Crystal Structures*, Bruker Analytical X-ray Instruments Inc., Madison, WI (1997).
[33] L.J. Farrugia. *J. Appl. Crystallogr.*, **30**, 565 (1997).
[34] L.J. Farrugia. *J. Appl. Crystallogr.*, **32**, 837 (1999).
[35] M.E. Reichmann, S.A. Rice, C.A. Thomas, P. Doty. *J. Am. Chem. Soc.*, **76**, 3047 (1954).
[36] K. Nakamoto. *Infrared and Raman Spectra of Inorganic and Coordination Compounds. Part B*, 5th Edn, p. 23, Wiley, New York (1997).
[37] A.B.P. Lever. *Inorganic Electronic Spectroscopy*, 2nd Edn, Elsevier, Amsterdam (1984).
[38] A.W. Addison, T.N. Rao, J. Reedijk, J. van Rijn, G.C. Verschoor. *J. Chem. Soc., Dalton Trans.*, 1349 (1984).
[39] S. Sen, S. Mitra, D.L. Hughes, G. Rosair, C. Desplanches. *Polyhedron*, **26**, 1740 (2007).
[40] B. Bussa, L.P. Sambasiva Rao, S. Muthukamalam, S. Ramachitra, S.S. Rani, T. Swu. *Synth. React. Inorg. Met.-Org. Nano-Met. Chem.*, **43**, 1073 (2013).
[41] B.J. Hathaway. *J. Chem. Soc., Dalton Trans.*, 1196 (1972).
[42] M. Jiang, Y.-T. Li, Z.-Y. Wu. *J. Coord. Chem.*, **65**, 1858 (2012).
[43] S. Thalamuthu, B. Annaraj, S. Vasudevan, S. Sengupta, M.A. Neelakantan. *J. Coord. Chem.*, **66**, 1805 (2013).
[44] P. Uma Maheswari, M. Palaniandavar. *J. Inorg. Biochem.*, **98**, 219 (2004).
[45] S. Roy, R. Banerjee, M. Sarkar. *J. Inorg. Biochem.*, **100**, 1320 (2006).
[46] J.B. Lepecq, C. Paoletti. *J. Mol. Biol.*, **27**, 87 (1967).
[47] Y.-G. Sun, K.-L. Li, Z.-H. Xu, T.-Y. Lv, S.-J. Wang, L.-X. You, F. Ding. *J. Coord. Chem.*, **66**, 2455 (2013).
[48] V.A. Joseph, K.M. Vyas, J.H. Pandya, V.K. Gupta, R.N. Jadeja. *J. Coord. Chem.*, **66**, 1094 (2013).
[49] Y.-J. Zheng, X.-W. Li, Y.-T. Li, Z.-Y. Wu, C.-W. Yan. *J. Coord. Chem.*, **65**, 3530 (2012).
[50] Z. Li-Hua, W. Wei-Na, W. Yuan, S. Guang. *J. Coord. Chem.*, **66**, 227 (2013).
[51] Z.B. Ou, Y.H. Lu, Y.M. Lu, S. Chen, Y.H. Xiong, X.H. Zhou, Z.W. Mao, X. Le. *J. Coord. Chem.*, **66**, 2152 (2013).
[52] F. Arjmand, M. Aziz, S. Tabassum. *Curr. Anal. Chem.*, **7**, 71 (2011).
[53] S. Banerjee, S. Sen, S. Basak, S. Mitra, D.L. Hughes, C. Desplanches. *Polyhedron*, **361**, 2707 (2008).
[54] D. Matoga, J. Szklarzewicz, W. Nitek. *Polyhedron*, **36**, 120 (2012).
[55] S.S. Mati, S. Roy, S. Chall, S. Bhattacharya, S.C. Bhattacharya. *J. Phys. Chem. B*, **117**, 14655 (2013).
[56] Q.-X. Wang, F. Gao, F. Gao, S.-X. Li, W. Weng, F.-Q. Liu, K. Jiao. *Biosens. Bioelectron.*, **32**, 50 (2012).
[57] S. Satyanarayana, J.C. Dabrowiak, J.B. Chaires. *Biochemistry*, **31**, 9319 (1992).
[58] J.M. Veal, R.L. Rill. *Biochemistry*, **30**, 1132 (1991).
[59] D. Sadhukhan, A. Ray, S. Das, C. Rizzoli, G.M. Rosair, S. Mitra. *J. Mol. Struct.*, **975**, 265 (2010).
[60] G.A.A. Al-Hazmi, M.S. El-Shahawi, I.M. Gabr, A.A. El-Asmy. *J. Coord. Chem.*, **58**, 713 (2005).
[61] A. Vijayaraj, R. Prabu, R. Suresh, C. Sivaraj, N. Raaman, V. Narayanan. *J. Coord. Chem.*, **64**, 637 (2011).